

Three-dimensional study of poly(lactic co-glycolic acid) micro-porous microspheres using hard X-ray nano-tomography

Dajiang Wang,^{a,‡} Na Li,^{b,‡} Zhili Wang,^a Kun Gao,^a Yongming Zhang,^{b,*} Yuyan Luo,^b Shengxiang Wang,^a Yuan Bao,^a Qigang Shao^a and Ziyu Wu^{a,c,*}

^aNational Synchrotron Radiation Laboratory, University of Science and Technology of China, 42 Hezuohua South Road, Hefei, Anhui 230029, People's Republic of China, ^bThe Third Affiliated Hospital of Sun Yat-sen University, 600 Tianhe Road, Guangzhou, Guangdong 510630, People's Republic of China, and ^cBeijing Synchrotron Radiation Facility, Institute of High Energy Physics, Chinese Academy of Sciences, Beijing 100049, People's Republic of China.

*E-mail: zhangym@tom.com, wuzy@ustc.edu.cn

Poly(lactic co-glycolic acid) (PLGA) is widely used in diverse fields, especially in delivering biologically active proteins and drugs. For these applications, the knowledge of morphology and microstructure of PLGA micro-porous microspheres is of great importance since they strongly influence the drug delivering efficiency. In this study, micro-porous PLGA microspheres loaded by bovine serum albumin are investigated by using a full-field Zernike phase contrast transmission hard X-ray microscope. From three-dimensional reconstructions and segmentations, fundamental microstructural parameters such as size, shape, distribution and volume ratio among pores and proteins inside PLGA microspheres were obtained. These parameters are useful to understand the relationship between the internal microstructure and drug encapsulation, as well as the drug release efficiency of PLGA microspheres. The presented results demonstrate the capability of hard X-ray nano-tomography to characterize porous microspheres loaded with proteins and drugs, and also open a way to analyse, optimize and design new PLGA microspheres for specific applications.

Keywords: hard X-ray imaging; nano-tomography; PLGA microspheres; salt concentration; drug delivery.

© 2014 International Union of Crystallography

1. Introduction

Since the first protein delivery experiment using polymers in 1976 (Langer & Folkman, 1976), various macromolecules have been developed to search for safe and efficient delivery systems for proteins and drugs (Drobnik, 1991; Kwon *et al.*, 1992; Grenha *et al.*, 2008). Poly(lactic co-glycolic acid) (PLGA) is a copolymer which is synthesized by two different monomers, glycolic acid (GA) and L-lactic acid (L-LA). The final products of PLGA *in vivo*, through the hydrolysis reaction, are two normal metabolites: carbon dioxide and water. Encapsulation of drugs in PLGA microspheres from which they are subsequently released at a controlled rate over a prolonged time allows a less frequent administration. The procedure increases patient compliance and reduces peak-related side effects by maintaining a stable drug level in the blood (Freiberg & Zhu, 2004). Due to its biodegradability and biocompatibility, the PLGA has been widely used as carrier in drug delivery systems and PLGA microspheres have been

for a long time one of the most important research systems to identify a reliable drug delivery system for bio-macromolecules such as peptides, proteins and vaccines (Wang *et al.*, 2004; Zhu *et al.*, 2000). The morphological internal structure of PLGA microspheres, *e.g.* porosity, plays a significant role in the release mechanism (Mao *et al.*, 2007). Therefore, quantitative information regarding the internal microstructures of intact microspheres is mandatory to build a mathematical model of a drug delivery process.

Many imaging techniques have been used to investigate the structure and function of the PLGA microspheres. However, almost all methods have been proved unsuitable for a non-destructive characterization of internal microstructures of intact PLGA microspheres. For example, light microscopy is widely used in many applications, but it has a low spatial resolution due to the diffraction limit. Electron microscopy can provide two-dimensional (2D) information of thin sections of samples with a high spatial resolution. However, it is very difficult to obtain three-dimensional (3D) information of intact PLGA microspheres since the penetration depth of electrons is extremely short. Recently, thanks to the progress

‡ These authors contributed equally to this work.

of X-ray optics, the transmission X-ray microscopy (TXM) based on synchrotron radiation bridged the gap between the light and the electron microscopy (Kagoshima *et al.*, 2002; Meirer *et al.*, 2011; Chao *et al.*, 2005). Nowadays, working at short wavelength and with accurate X-ray optics, TXM may achieve a spatial resolution up to 26 nm (Yuan *et al.*, 2012; Schneider *et al.*, 2010). Due to the high penetration power and large depth of focus of X-rays, TXM nano-tomography can provide 3D internal structure information of intact large samples with thicknesses up to 60 μm (Zhang *et al.*, 2013). Using the Zernike phase contrast, the high image contrast of TXM nano-tomography enables the visualization of 3D structures of low-absorbing samples, such as biological tissues, organic materials and soft matter (Wang *et al.*, 2013; Mizutani *et al.*, 2007; Tian *et al.*, 2008; Luning *et al.*, 2007).

In this work, we investigated the 3D microstructure of PLGA microspheres using the transmission hard X-ray microscope at BSRF operated in the large field-of-view mode. The 3D reconstruction provided fundamental structural parameters such as size, shape, distribution, volume ratio among pores and proteins inside the PLGA microspheres. These parameters are useful to understand the relationship between internal microstructures and drug delivery efficiency of PLGA microspheres.

2. Materials and methods

PLGA (50:50, inherent viscosity 0.85 dL g⁻¹ in CHCl₃) was purchased from Birmingham Polymer (USA). Poly(vinyl-alcohol)124 (PVA124, MW 85, 124 kDa, 98–99% hydrolyzed) was supplied by Shanghai Zhanyun. Fluorescein isothiocyanate bovine serum albumin (BSA-FITC) was purchased from Genview (USA). Sodium alginate (Protanal LF 200DL) was purchased from FMC BioPolymer. All the other reagents were of analytical grade.

2.1. Preparation of PLGA microspheres

PLGA microspheres were prepared by a modified (W1/O/W2) double emulsion method. Briefly, BSA was dissolved in 0.3 ml alginate solution containing F68 and NaCl (the dose used to prepare microspheres No. 1, No. 2 and No. 3 were 1.5 mg, 3 mg and 6 mg, respectively) and emulsified with 4 ml organic solution (15% PLGA in CH₂Cl₂) by homogenizing to form the primary emulsion. The primary emulsion was injected into an aqueous phase containing PVA and CaCl₂, and then homogenized to produce the double W/O/W emulsion. The resultant emulsion was transferred to the solvent extraction phase containing PVA and CaCl₂ to allow microspheres hardening by stirring at 400 r.p.m. for 3 h. The hardened microspheres were centrifuged, washed three times with water, freeze-dried, and stored under desiccant at 253 K. 20 mg of PLGA microspheres were mixed with 1 ml of 2.5% glutaraldehyde in 0.1 M PBS for 4 h at 277 K, rinsed in PBS buffer three times, dehydrated in a graded ethanol series of 30–100% concentration, stained with 1 ml of 2% uranyl

acetate (in ethanol) for 4 h and finally rinsed in the PBS buffer three times (Zhao & Rodgers, 2006).

2.2. TXM nano-tomography

The nano-tomography experiments were carried out using the transmission hard X-ray microscope, located at the BSRF 4W1A beamline (Yuan *et al.*, 2012). In our experiments the photon energy was fixed at 8 keV. The elliptically shaped capillary condenser focuses the incident X-rays onto the sample, then the sample image is magnified 11 \times with an objective zone-plate located 79 mm from the sample. The diameter and outermost zone width of the objective zone-plate was 320 μm and 35 nm, respectively. A phase ring was placed in the back focal plane of the objective zone-plate to provide Zernike phase contrast. Located 900 mm from the sample, a 1024 \times 1024 charge coupled device (CCD) camera with 0.65 μm pixel size recorded the sample image. After the scintillation crystal transformed X-rays into visible light, the CCD displayed the sample image with a 20 \times optical magnification. Under this operation mode, the resolution reached 100 nm as tested by gold spoke patterns (Zhang *et al.*, 2013), and the corresponding field-of-view (FOV) was 60 μm \times 60 μm , *i.e.* the large FOV mode.

In order to improve the image contrast of BSA, the samples were stained with heavy metals. In addition, TXM was operated in Zernike phase contrast mode (Yang *et al.*, 2010). Three PLGA microspheres prepared with different formulations were picked out and glued on the top of the pin, which was fixed on the sample holder. A series of 361 sequential projective images with 128 nm pixel size (binning 2, 512 \times 512) were collected at angles from -90° to $+90^\circ$ with an angular step of 0.5° . With an exposure time of 20 s for each image, the total time required to collect the tomographic data was about 2 h for each microsphere. The 3D reconstruction of the PLGA microspheres was performed by a standard filtered back-projection algorithm (Kak & Slaney, 1988). Three-dimensional rendering and segmentation were performed by using commercial software (*Amira 5.4.2*; VSG).

3. Results and discussion

To obtain the morphology of the PLGA microspheres, we first investigated the PLGA microspheres *via* a scanning electron microscope (SEM), and the results are shown in Fig. 1. As shown in Fig. 1(a), the PLGA microspheres synthesized by the modified (W1/O/W2) double emulsion method were spherical with a few pores in the range of 1–3 μm on the surface. Fig. 1(b) indicates that the PLGA microspheres had a high internal porosity with pores ranging from 1 to 10 μm . The porosity here was employed to describe the internal morphology of the PLGA microsphere, which is defined as the total volume of pores divided by that of the PLGA microsphere. However, the SEM results are not sufficient to provide quantitative microstructural information of PLGA microspheres, such as the volume, shape and distribution of pores. The connection among pores is not clear either. Moreover, the

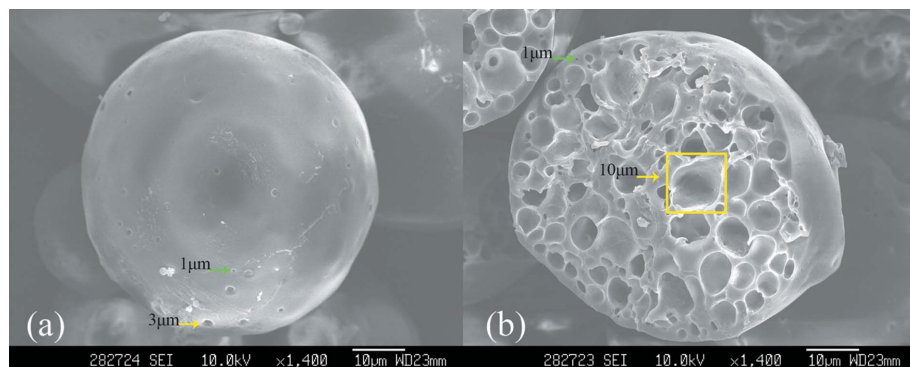


Figure 1 Scanning electron microscopy images. Surface (a) and internal (b) morphology of a PLGA microsphere. The smallest and biggest pores are marked by green and yellow arrows, respectively.

SEM sectioning of samples is destructive, resulting in a severe deformation of microsphere edges, as can be seen from Fig. 1(b).

By introducing heavy metal staining and Zernike phase contrast, 3D microstructural information of the PLGA microspheres can be visualized and quantified using TXM nano-tomography. Fig. 2 shows a high contrast projective image of the PLGA microsphere No. 1, where the gold nanoparticle marked by the yellow arrow has been used to align projective images. The observed intensity of each pixel in Fig. 2 contains both amplitude and phase information. The projective image taken at 8 keV shows a good contrast and the overlapping structures of pores can be clearly recognized. Indeed, the internal fine structure of the PLGA microspheres cannot be clearly identified by a single 2D projection. The overlap of complex features in projections makes the image analysis difficult. In order to distinguish precisely the internal structure of PLGA microspheres, both 3D reconstruction and rendering are necessary. Fig. 3 shows a virtual cross section of the PLGA microsphere No. 1 from the 3D reconstruction, in which the internal pores can be clearly distinguished and BSA, marked by the yellow arrow, is recognized on the inner walls of pores. Moreover, we can recognize that the pores have

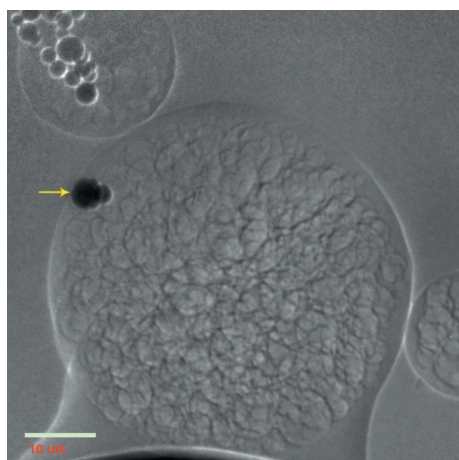


Figure 2 TXM projective image of a PLGA microsphere. A gold nanoparticle marked by the yellow arrow has been used for the alignment procedure.

bright boundaries surrounding their peripheries, the so-called ‘halo effect’ due to the phase contrast (Youn & Jung, 2006). The halo effect is usually observed at the edge between two regions where the refractive indices are different. In our images, the bright areas due to the halo effect appear outside pores. Thus, these phase contrast results clearly point out internal microstructures of PLGA microspheres.

The 3D rendering of the PLGA microspheres was obtained by drawing the contour of the microspheres and pores according to clear boundaries for each reconstruction slice. Inside the

pores, every binary voxel with a grey value between 0 and 40 was set to BSA. Accordingly, in Fig. 4, we may recognize size, shape and distribution of both pores and BSA. Imaging results confirmed that the PLGA microspheres were spheres with a diameter of about 50 μm. They had a high internal porosity, with pore sizes ranging from 2 to 10 μm. As shown in Fig. 4, we observed an increase in pore size, pore size distribution, porosity and BSA content from the microspheres No. 1 to No. 3. The pore slice movies (Videos 1, 2 and 3 of the supporting material) of the three microspheres show the porosity variation visually.

Structural parameters of microspheres are listed in Table 1. The porosity increases from 19.94% of microsphere No. 1 to 44.76% of microsphere No. 3. This variation can be explained by the gradually increased salt concentration from microsphere No. 1 to microsphere No. 3 in the preparation process. The organic phase of the modified (W1/O/W2) double emulsion acts as a semi-permeable membrane. It allows water across the organic phase under the influence of an osmotic gradient. Before microspheres harden completely, higher salt concentration in W1 leads more water to pass from the

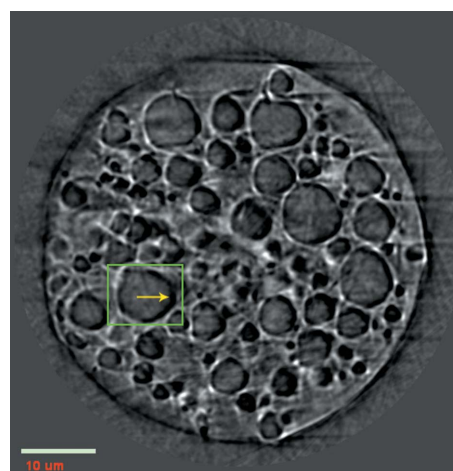


Figure 3 Virtual cross section of a PLGA microsphere obtained from the TXM nano-tomography reconstruction. A cross section of the pore is inside the green square where the dark halo marked by the yellow arrow is the BSA stuck to the inner wall of the pore.

Table 1

Summary of microstructural parameters measured from 3D reconstructions of three microspheres.

	Microsphere		
	No.1	No.2	No.3
Volume of BSA (μm^3)	4333	10918	11826
Volume of pore (μm^3)	12332	18856	31746
Volume of microsphere (μm^3)	61859	73890	70932
Volume fraction of BSA	7.00%	14.77%	16.67%
Porosity	19.94%	25.52%	44.76%
Surface area/volume of pore (μm^{-1})	0.44	0.58	0.76

external to the internal phase along with the osmotic gradient. The expansion of the internal droplets results in the increase of porosity and pore size after microspheres hardened. Meanwhile, the expansion of the internal phase causes the instability of the W1/O/W2 double emulsion, resulting in a release of the internal phase into the external phase and a loss of BSA during encapsulation (Pistel & Kissel, 2000). This process explains the increase of the BSA content from the microspheres No. 1 to No. 3, and the increase rate is lower compared with that of the porosity.

In order to understand how pores affect the drug encapsulation efficiency, a relationship between pore size and BSA volume was obtained. Assuming an ideal spherical shape, the diameter was used to represent the pore size. Some pores were picked out randomly from 2 to 10 μm to calculate the volume ratio between BSA and pores. As presented in Fig. 5, the data of all three microspheres point out that the smaller the pore

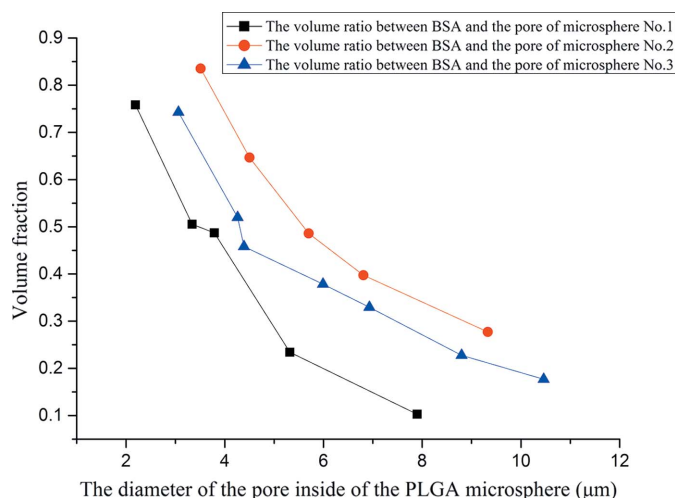


Figure 5

Curves of the volume ratio between BSA and pores in the three microspheres.

then the higher the protein loaded amount. In particular, when the diameter of the pore is below 4 μm , more than 50% of the internal space is occupied by proteins. All the above results suggest that the drug encapsulation efficiency is concerned not only with pore size but also with microsphere formula, and the drug delivery dose can be precisely controlled by adjusting the formula of the PLGA microsphere synthesized by the modified (W1/O/W2) double emulsion method.

4. Conclusion

In this study, we measured critical microstructural parameters and reconstructed the 3D internal microstructure of PLGA microspheres by using the hard X-ray microscope at BSRF. The reconstruction reveals a quantitative relationship between microstructures and drug encapsulation efficiency of PLGA microspheres. Besides, this research also demonstrates that transmission hard X-ray microscopy is well suited to investigate 3D microstructures of PLGA microspheres, since it can provide quantitative 3D data with a high spatial resolution. We believe that the technique will help to analyse, optimize and design new PLGA microspheres for special applications in the future.

This work was partly supported by the National Basic Research Program of China (2012CB825801), the Science Fund for Creative Research Groups (11321503), the Knowledge Innovation Program of the Chinese Academy of Sciences (KJCX2-YW-N42), the National Natural Science Foundation of China (11205157, 11205189, 11305173), the China Postdoctoral Science Foundation (2013T60626), Science and Technology Major Projects of Guangdong Province (2011A080504003).

References

Chao, W. L., Harteneck, B. D., Liddle, J. A., Anderson, E. H. & Attwood, D. T. (2005). *Nature (London)*, **435**, 1210–1213.
 Drobniak, J. (1991). *Adv. Drug Deliv. Rev.* **7**, 295–308.

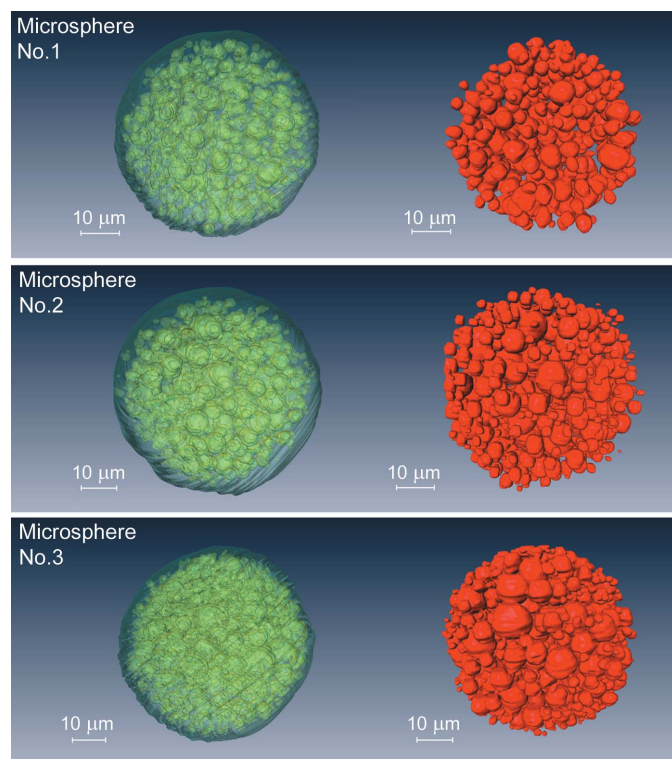


Figure 4

3D rendering of BSA and pores inside the PLGA microspheres. In the three panels BSA is in yellow, cyan is the external surface of a PLGA microsphere while pores are in red.

- Freiberg, S. & Zhu, X. X. (2004). *Intl J. Pharm.* **282**, 1–18.
- Grenha, A., Remuñán-López, C., Carvalho, E. L. S. & Seijo, B. (2008). *Eur. J. Pharm. Biopharm.* **69**, 83–93.
- Kagoshima, Y., Yokoyama, Y., Ibuki, T., Niimi, T., Tsusaka, Y., Takai, K. & Matsui, J. (2002). *J. Synchrotron Rad.* **9**, 132–135.
- Kak, A. C. & Slaney, M. (1988). *Principles of Computerized Tomographic Imaging*. New York: IEEE Press.
- Kwon, G. S., Bae, Y. H., Cremers, H., Feijen, J. & Kim, S. W. (1992). *Intl J. Pharm.* **79**, 191–198.
- Langer, R. & Folkman, J. (1976). *Nature (London)*, **263**, 797–800.
- Luning, K., Pianetta, P., Yun, W. B., Almeida, E. & van der Meulen, M. (2007). *AIP Conf. Proc.* **879**, 1333–1336.
- Mao, S. R., Xu, J., Cai, C. F., Germershaus, O., Schaper, A. & Kissel, T. (2007). *Intl J. Pharm.* **334**, 137–148.
- Meirer, F., Cabana, J., Liu, Y., Mehta, A., Andrews, J. C. & Pianetta, P. (2011). *J. Synchrotron Rad.* **18**, 773–781.
- Mizutani, R., Takeuchi, A., Hara, T., Uesugi, K. & Suzuki, Y. (2007). *J. Synchrotron Rad.* **14**, 282–287.
- Pistel, K. F. & Kissel, T. (2000). *J. Microencapsul.* **17**, 467–483.
- Schneider, G., Guttman, P., Heim, S., Rehbein, S., Mueller, F., Nagashima, K., Heymann, J. B., Müller, W. G. & McNally, J. G. (2010). *Nat. Methods*, **7**, 985–987.
- Tian, Y. C., Li, W. J., Chen, J., Liu, L. H., Liu, G., Tkachuk, A., Tian, J. P., Xiong, Y., Gelb, J., Hsu, G. & Yun, W. B. (2008). *Rev. Sci. Instrum.* **79**, 103708.
- Wang, C., Ge, Q., Ting, D., Nguyen, D., Shen, H. R., Chen, J. Z., Eisen, H. N., Heller, J., Langer, R. & Putnam, D. (2004). *Nat. Mater.* **3**, 190–196.
- Wang, Z. L., Gao, K., Chen, J., Hong, Y. L., Ge, X., Wang, D. J., Pan, Z. Y., Zhu, P. P., Yun, W., Jacobsen, C. & Wu, Z. Y. (2013). *Biotechnol. Adv.* **31**, 387–392.
- Yang, Y., Li, W., Liu, G., Zhang, X., Chen, J., Wu, W., Guan, Y., Xiong, Y., Tian, Y. & Wu, Z. (2010). *J. Microsc.* **240**, 14–20.
- Youn, H. S. & Jung, S. W. (2006). *J. Microsc.* **223**, 53–56.
- Yuan, Q., Zhang, K., Hong, Y., Huang, W., Gao, K., Wang, Z., Zhu, P., Gelb, J., Tkachuk, A., Hornberger, B., Feser, M., Yun, W. & Wu, Z. (2012). *J. Synchrotron Rad.* **19**, 1021–1028.
- Zhang, K., Li, D. E., Hong, Y. L., Zhu, P. P., Yuan, Q. X., Huang, W. X., Gao, K., Zhou, H. Z. & Wu, Z. Y. (2013). *Chin. Phys. B*, **22**, 076801.
- Zhao, A. Y. & Rodgers, V. G. J. (2006). *J. Control. Release*, **113**, 15–22.
- Zhu, G. Z., Mallery, S. R. & Schwendeman, S. P. (2000). *Nat. Biotechnol.* **18**, 52–57.